Journal of Materials Chemistry C

ROYAL SOCIETY OF CHEMISTRY

PAPER

View Article Online
View Journal | View Issue

Cite this: J. Mater. Chem. C, 2025, 13, 19408

A strongly birefringent sulfate crystal with a wide second-harmonic generation phase-matching range

Zhiyong Bai,[ac] Shanshan Chen,[a] Xu Chen,[a] Yong Wang,[a] Xinwei Zhou,[ac] Yipeng Song,[ac] Yanqiang Li,[a] Sangen Zhao *[b] and Junhua Luo *[ac]

Received 7th June 2025,
Accepted 1st August 2025

DOI: 10.1039/d5tc02204e

rsc.li/materials-c

Birefringence is pivotal for the improvement of the conversion efficiency of nonlinear optical (NLO) materials *via* phase matching (PM). The engineering of proper birefringence for short-wavelength ultraviolet (UV) NLO crystals, particularly for those based on homoleptic tetrahedral moieties, such as sulfates, remains challenging, mainly because of the conflicting correlation of energy bandgap and birefringence. We herein synthesized a short-wavelength UV NLO sulfate, $Li_2SO_4{\cdot}C_2H_5NO_2$ (LSG), composed of homoleptic $[SO_4]^{2-}$ tetrahedra and π-conjugated zwitterionic glycine. To our surprise, both experimental and theoretical studies indicate that LSG is strongly birefringent, with an experimental birefringence of 0.144 at 550 nm. Benefiting from its satisfactory birefringence, LSG exhibited desirable PM behavior in the UV regime with a type-I PM wavelength of 262 nm. Powder second harmonic generation (SHG) measurements revealed that LSG can achieve PM under 1064 and 532 nm with an efficiency that is 0.7 and 0.3 times that of KDP and β-BBO, respectively, underscoring its potential application in generating UV laser by a direct SHG process. LSG simultaneously maintained a wide UV transparency window, with an optical bandgap of 5.20 eV and a short UV cutoff edge of 220 nm, as well as high thermal stability that is comparable to benchmark KDP. Structure-performance relationship investigation clearly indicated that the π-conjugated glycine component is mainly responsible for these crucial properties.

Introduction

Nonlinear optical (NLO) materials are of great importance in laser science and technology as they can expand the wavelength range of common laser sources by a frequency conversion process, such as second-harmonic generation (SHG).[1–6] Over the past decades, the search for short-wavelength UV NLO crystals has largely focused on π-conjugated borates, with the widely applicable β-BBO (β-BaB_2O_4), LBO (LiB_3O_5), and CLBO ($CsLiB_6O_{10}$) as outstanding representatives.[7–11] Nevertheless, the exploration of new candidates is still of intense interest as some drawbacks exist for these commercially applicable materials.[12–21]

It is well known that promising short-wavelength UV NLO materials should satisfy a few tough performance requirements, including a broad UV transmission window, suitable birefringence for phase-matching, relatively large SHG effects as well as other physical and chemical properties. Benefiting from the wide UV transmission window, in recent years, sulfate crystals, such as $NH_4NaLi_2(SO_4)_2$, $(NH_4)_2Na_3Li_9(SO_4)_7$, $Li_9Na_3Rb_2(SO_4)_7$, $LiRb_4[B(SO_4)_4]$, $LiNH_4SO_4$, and $LaNH_4(SO_4)_2$, have attracted increasing attention as short-wavelength UV NLO crystals.[22–29] However, analogous to phosphates, the broad applicability of sulfate crystals can be hindered by their low birefringence arising from homoleptic $[SO_4]^{2-}$ tetrahedra with weak anisotropy. Three main approaches have been developed to enhance the birefringence of sulfate crystals.

(1) The first route involves the introduction of cations that are prone to forming highly distorted polyhedra, such as Sb^{3+}, Bi^{3+}, Hg^{2+}, Zr^{4+}, and Hf^{4+}. The implementation of this strategy has led to the discovery of a number of optical sulfate crystals with a notable rise in birefringence, such as $CsSbF_2SO_4$,[30] $A_2Bi_2(SO_4)_2Cl_4$ (A = K, Rb, and NH_4),[31] $HgSO_4$,[32] $Hg_3O_2SO_4$,[33] MF_2SO_4 (M = Ce, Zr, and Hf),[34,35] and $Hg_4(Te_2O_5)(SO_4)$.[36]

(2) The second route involves the development of new heteroleptic tetrahedra groups, such as $[SO_3F]^-$, $[NH_2SO_3]^-$, and $[CH_3SO_3]^-$, by chemically tailoring homoleptic $[SO_4]^{2-}$. The partial replacement of the O atom in $[SO_4]^{2-}$ by F, NH_2, and CH_3 with different chemical properties allows for the enhancement of polarizability anisotropy and thus results in birefringence gain.

[a] State Key Laboratory of Functional Crystal and Devices, Fujian Institute of Research on the Structure of Matter, Chinese Academy of Sciences, Fuzhou 350002, China. E-mail: jhluo@fjirsm.ac.cn
[b] Quantum Science Center of Guangdong-Hong Kong-Macao Greater Bay Area (Guangdong), Shenzhen, 518045, China. E-mail: zhaosangen@quantumsc.cn
[c] University of Chinese Academy of Sciences, Beijing 100049, China

Resultant optical materials include fluoroxosulfates,[37] $M(NH_2SO_3)_2$ (M = Ba and Sr),[38] $Cs_2Mg(NH_2SO_3)_4{\cdot}4H_2O$,[39] $Ba(CH_3SO_3)_2$,[40] among others.

(3) Incorporating planar π-conjugated units is also an effective way. A huge discrepancy in polarizability can occur along the direction parallel and perpendicular to the plane of the planar π-conjugated groups, which is quite beneficial for birefringence enhancement, as exemplified by the recently discovered $(NH_4)_2B_4SO_{10}$[41] and $K(3\text{-}C_5H_4NSO_3)$.[42] Moreover, the richness and diversity of π-conjugated groups (especially the organic ones) endow this approach with great potential in tuning the birefringence of sulfate crystals. Compared to the first two routes, applying this strategy to develop short-wavelength UV NLO sulfates is the least explored. The challenges probably come from achieving a balance between broad UV transmission and sufficient birefringence. Our previous studies have revealed that the simplest amino acid, glycine, might be a good choice for realizing such a balance, which is attributable to the following merits.[43] Firstly, the presence of the π-conjugated carboxyl in glycine favors the enhancement of the birefringence. Secondly, glycine-based compounds are UV-transparent and have a strong affinity to form co-crystals with inorganic compounds. With these considerations in mind, we successfully synthesized the co-crystal compound of Li_2SO_4 and glycine, namely $Li_2SO_4{\cdot}C_2H_5NO_2$ (LSG). Although an earlier report[44] mentioned that this compound is NLO-active, its birefringence and phase-matchability performances, which are important indicators that can determine whether the crystal can be practically applicable, are still unknown. In this study, both theoretical and experimental tools have been applied to study its birefringence, PM behavior, phase-matchable SHG, UV transmission, and structure–property relationship. Our results have shown that LSG is strongly birefringent, with a large birefringence value of 0.144@550 nm. Notably, the birefringence of LSG is much higher than that of pure sulfate crystals; for example, its birefringence is *ca.* 36 times that of the Li_2SO_4 crystal, highlighting the neglected role of glycine in birefringence properties. It maintained a broad transmission window at the UV side, including a wide energy band gap of 5.20 eV and a short UV cut-off edge of 220 nm. Moreover, the powder SHG test indicated that it is phase-matchable under both 1064 and 532 nm light, underscoring its potential for generating a UV laser by a direct SHG process.

Experimental section

Synthesis of LSG

The raw materials glycine (99%, Adamas) and Li_2SO_4 (99%, Aladdin) were used as received. The stoichiometric glycine and Li_2SO_4 were dissolved in deionized water. After stirring and heating for 30 minutes, a clear solution was obtained. The obtained solution was evaporated at a constant temperature of 318 K. Colorless, centimeter-sized single crystals were formed in a few days.

Powder X-ray diffraction (PXRD)

The PXRD test was carried out at room temperature on a Rigaku MiniFlex 600 diffractometer equipped with Cu Kα radiation (λ = 1.5406 Å). The 2θ range was 10–60° with a scan step width of 0.02° and a fixed counting time of 5 s per step.

Single-crystal structure determination

The single crystal X-ray diffraction data were collected on a Bruker APEX-III CCD diffractometer equipped with Mo Kα radiation (λ = 0.71073 Å). Data reduction, cell refinement, and absorption corrections were conducted using the program APEX4. The structure was solved by the intrinsic phasing method and refined on F^2 by full-matrix least-squares techniques using the program Olex2 supplemented by the SHELXT and SHELXL.[45–47] The structure was checked using the program PLATON,[48] and no higher symmetry was found. Crystal data and structure refinement are given in Table S1. Atomic coordinates, isotropic displacement parameters, bond lengths/angles, and hydrogen bonds are listed in Tables S2–S5.

Ultraviolet-visible (UV-vis) spectroscopy

The UV-vis reflectance spectrum was collected on a Lambda-950 UV/Vis/NIR spectrophotometer in the wavelength range of 200–900 nm. In order to determine the band gap, the diffuse reflectance spectral data were subsequently converted to the function of reflectance using the Kubelka–Munk function:[49]

$$F(R) = (1 - R)^2/2R = K/S$$

where R denotes the reflectance, K the absorption coefficient, and S the scattering factor. In the $F(R)$ *versus* E (eV) plot, extrapolating the linear part of the rising curve to zero provides the onset of the absorption.

The UV-vis transmittance spectrum was recorded on a Lambda-950 UV/Vis/NIR spectrophotometer in the wavelength range of 200–800 nm. The single crystal of LSG was hand-polished before measurement.

Thermal stability

The thermal stability was investigated by differential thermal analysis (DTA) on a simultaneous NETZSCH STA 449C thermal analyzer in an atmosphere of flowing N_2. About 6 mg of LSG powder was loaded into an Al_2O_3 crucible, heated at a rate of 10 K min^{-1} from room temperature to 1273 K.

Birefringence measurement

The birefringence of LSG was determined on a NIKON ECLIPSE LV100N POL polarizing microscope equipped with a Berek compensator. The average wavelength of the light source was 550 nm. The formula for calculating the birefringence is given below:

$$R = |N_g - N_p| \times d = \Delta n \times d$$

Here, R represents the retardance; N_g, N_p, and Δn stand for the refractive index of fast light, slow light, and the birefringence, respectively, and d is the thickness of the crystal.

Computation method

The electronic structures and optical properties were performed using a plane-wave basis set and pseudo-potentials within density functional theory (DFT) implemented in the total-energy code CASTEP.[50] For the exchange and correlation

function, Perdew–Burke–Ernzerhof in the generalized gradient approximation was chosen.[4] The interactions between the ionic cores and the electrons were described by the norm-conserving pseudopotential.[51] The following valence-electron configurations were considered in the computation: Li-$1s^2 2s^1$, S-$3s^2 3p^4$, C-$2s^2 2p^2$, N-$2s^2 2p^3$, O-$2s^2 2p^4$, and H-$1s^1$. The number of plane waves included in the basis sets was determined by a cutoff energy of 750 eV. The numerical integration of the Brillouin zone was performed using a Monkhorst–Pack *k*-point mesh of 2 × 7 × 4. The other parameters and convergent criteria kept the default values of the CASTEP code. The polarizability anisotropy of the mentioned groups was calculated using the DFT method implemented by the Gaussian09w package at the RB3LYP/6-31G level.[52] The models were optimized before calculation.

Results and discussion

Synthesis and characterization

LSG was synthesized from an aqueous solution containing stoichiometric Li_2SO_4 and $C_2H_5NO_2$ (Fig. 1a). Colorless block-shaped single crystals of LSG were harvested by evaporating the solution at 45 °C over a few days (Fig. S1). Powder X-ray diffraction (PXRD) confirmed the phase purity (Fig. S2). After exposure in air for 3 months, LSG still showed PXRD patterns identical to the fresh samples, indicating that it is stable in air and non-hygroscopic (Fig. S2). The TG analysis revealed that LSG is thermally stable up to 566 K; above this temperature, it decomposes by releasing the organic glycine (Fig. S3). Note that the thermal stability of LSG is comparable to that of KDP (525 K), and much higher than that of the well-known semi-organic NLO material LAP (385 K),[53] as well as newly discovered $(C_5H_6ON)^+(H_2PO_4)^-$ (439 K),[53] $[C(NH_2)_3]_2[B_3O_3F_4(OH)]$ (418 K),[54] and $C(NH_2)_3SO_3F$ (435 K),[55] *etc.* In the structure, the carboxyl groups in glycine are tightly bonded to the Li atom by forming Li–O bonds (see the crystal structure section), which is probably responsible for the high thermal stability of LSG.

Crystal structure

LSG crystallizes in the non-centrosymmetric polar $Pna2_1$ space group with the orthorhombic lattice constants a = 16.3528(8) Å, b = 4.9908(2) Å, c = 7.6292(4) Å, V = 622.65(5) Å,^{3} and Z = 4 (Table S1). The asymmetric unit consists of one unique S, two Li, four O atoms, and a complete $C_2H_5NO_2$ molecule. The S atom is surrounded by four O atoms, forming $[SO_4]^{2-}$ tetrahedra with S–O bond lengths ranging from 1.4638(19) to 1.4870(3) Å and O–S–O bond angles in the range of 108.22(18)–110.90(11) (Fig. 1d). Both Li(1) and Li(2) atoms are 4-coordinated to yield $[LiO_4]^{7+}$ tetrahedra. The Li–O bond distances and O–Li–O bond angles vary from 1.8720(7) to 1.9720(8) Å and 105.2(4)° to 113.8(3)°, respectively. $C_2H_5NO_2$ is zwitterionic. LSG adopts a layered structure with the

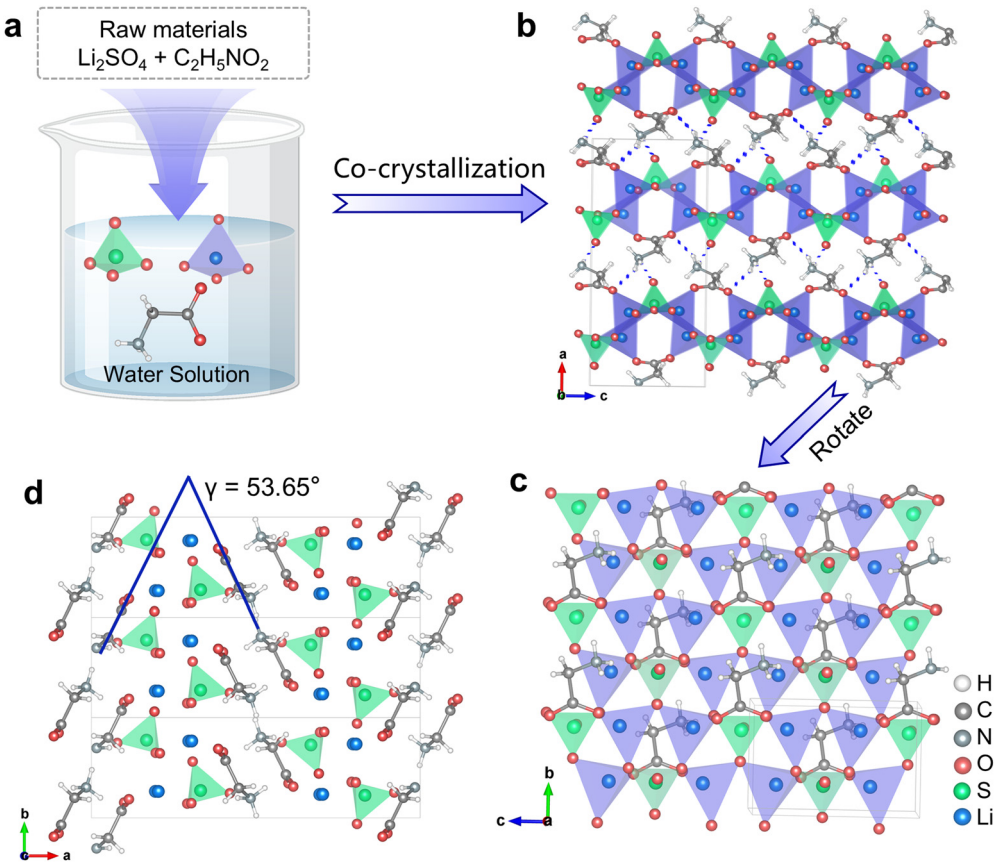

Fig. 1 (a) LSG was synthesized through the co-crystallization of stoichiometric Li_2SO_4 and $C_2H_5NO_2$ in aqueous solution. (b) The layered structure of LSG. (c) The $[Li_2SO_4(C_2H_5NO_2)]$ single layer. (d) The arrangement of $C_2H_5NO_2$.

2D layers stacked along the *a*-axis and strengthened by hydrogen bonding (Fig. 1b and Table S7). The single layer $[Li_2SO_4(C_2H_5NO_2)]$ is built up by alternatively connected $[Li(SO_4)_3(C_2H_5NO_2)]$ clusters composed of one $[LiO_4]^{7+}$, three $[SO_4]^{2-}$ and one $C_2H_5NO_2$ molecule by corner-sharing (Fig. 1c). There are two groups of $C_2H_5NO_2$ molecules, and they exhibit a dihedral angle of $\gamma = 53.65^\circ$ (Fig. 1d).

Optical transparency

The UV-Vis diffuse reflectance spectrum was obtained based on LSG powders (Fig. 2a). The results show that LSG has a short absorption edge of 210 nm, indicating that LSG is UV transparent. The value corresponds to the optical band gap (E_g) 5.20 eV, determined from the Kubelka–Munk function. To obtain an accurate transmittance cut-off edge ($\lambda_{cut\text{-}off}$) at the UV side, the UV-visible transmittance spectrum was further recorded using a hand-polished crystal wafer (Fig. 2b and inset). LSG showed high transmittance from 250 to 800 nm, and $\lambda_{cut\text{-}off}$ was determined to be 220 nm.

NLO measurements

The SHG capability of LSG was examined by the Kurtz-Perry method with incident laser wavelengths of 1064 and 532 nm. The standard NLO crystals KDP and β-BBO were used for comparison. As displayed in Fig. 2c and d, the SHG intensity of LSG under both 1064 nm and 532 nm light increased with increasing grain sizes before they attained the maximum, independent of the particle size, which indicates that LSG is phase-matchable under both 1064 nm and 532 nm light. The SHG efficiencies of LSG were 0.7 × KDP and 0.3 × β-BBO at their respective largest particle sizes. Such a powder SHG efficiency is comparable to a few NLO sulfates, such as $BeSO_4{\cdot}4H_2O$ (0.6 × KDP), $(NH_4)_2Na_3Li_9(SO_4)_7$ (0.5 × KDP),[25] $NH_4NaLi_2(SO_4)_2$ (1 × KDP),[25] $Li_{2.9}Cs_{1.1}(SO_4)_2$ (0.8× KDP),[56] $LiNH_4(SO_4)_2$ (0.85 × KDP),[29] $LiRb_4[B(SO_4)_4]$ (1 × KDP),[28] and $(NH_4)_2B_4SO_{10}$ (1.1 × KDP and 0.15 × β-BBO).[41] The second-order NLO coefficients d_{ij} of LSG were calculated based on the density functional theory (DFT) method. Considering the restriction of the $Pna2_1$ space group (point class: *mm*2) and Kleinman's symmetry, LSG exhibits three non-vanishing independent SHG tensors, $d_{15} = d_{31} = -0.024$ pm V^{-1}, $d_{24} = d_{32} = 0.293$ pm V^{-1}, and $d_{33} = -0.310$ pm V^{-1}. Among these, d_{24} and d_{33} (absolute value) are approximately 0.8 times that of $d_{36} = 0.39$ pm V^{-1} of standard KDP, which is in accordance with the experimental results.

Birefringence and phase-matching properties

The powder SHG examination revealed that LSG is phase-matchable at 532 nm, which suggests that it probably has enhanced birefringence. We first conducted polarization-resolved optical microscopy (PROM) to qualitatively study the optical anisotropy of LSG. As shown in Fig. 3, the single crystal of LSG showed an interference color (purple in this case) under cross-polarization light, which periodically changed from the brightest to darkest with every single rotation angle of 45°,

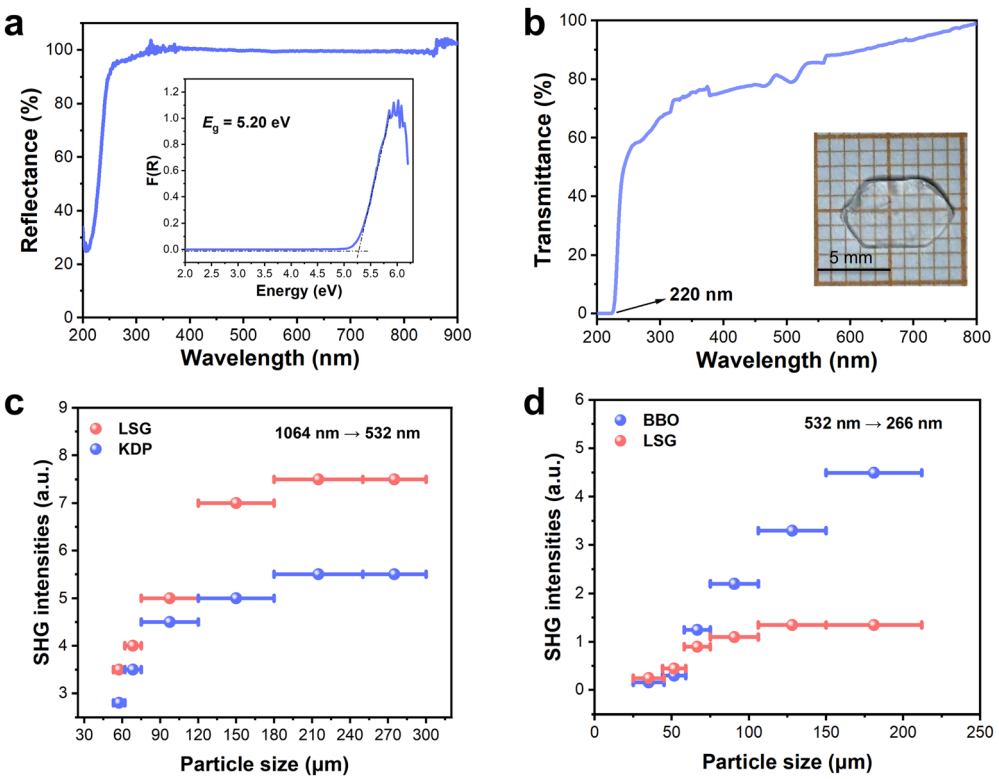

Fig. 2 The optical transparency and SHG response of LSG. (a) UV-vis diffuse reflectance spectrum (inset: optical bandgap determined from the Kubelka–Munk function). (b) UV-vis transmittance spectrum based on a hand-polished single crystal (inset: the crystal image used for data collection). The particle-size-dependent powder SHG response of LSG measured at (c) 1064 nm and (d) 532 nm.

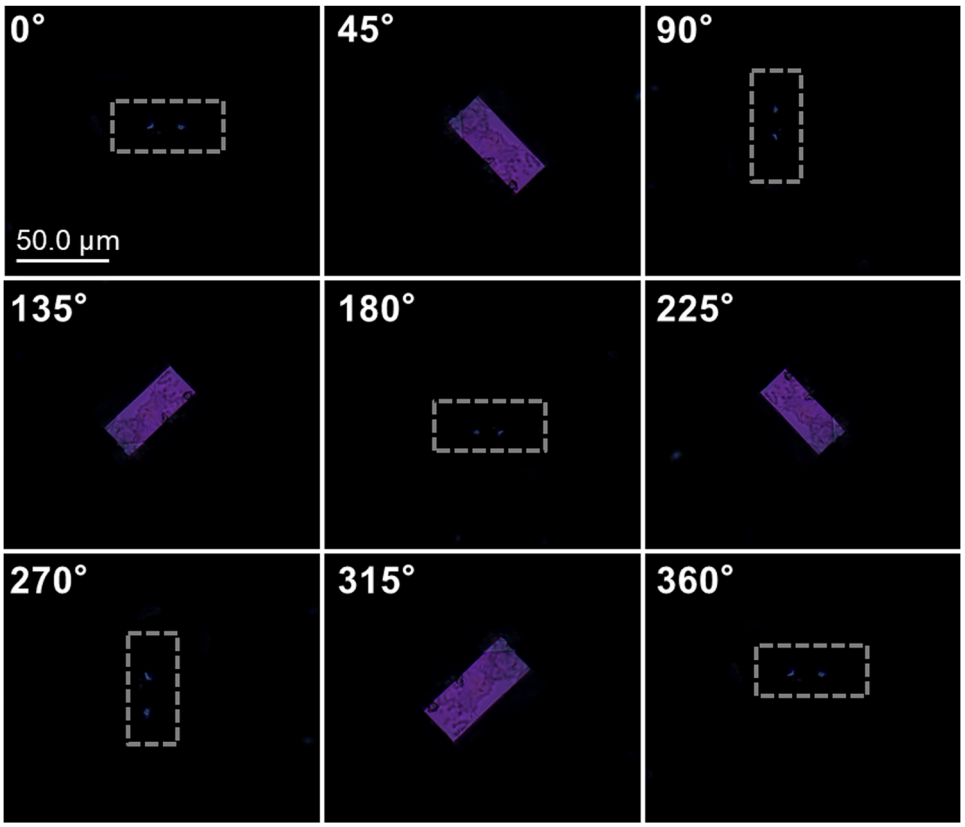

Fig. 3 Transmission polarization-resolved optical images of the LSG single crystal under cross-polarized light, varying with the rotation angle. The scale bar applies to all images.

indicating that LSG is optically anisotropic, *i.e.*, birefringent. The quantitative determination of the birefringence value of LSG was based on a polarizing microscope equipped with the Berek compensator, which has been widely applied to study the birefringence property of many compounds.[57–59] A naturally developed single crystal wafer showing a pink interference color under cross-polarized light was first selected (Fig. 4a). By adjusting the Berek compensator, the pink color changed to dark, indicating that the crystal achieved complete extinction (Fig. 4b). The final retardation (R) was 2.115 μm, and the thickness (d) of the crystal sample was measured to be 68.6 μm (Fig. 4c). Based on the equation $\Delta n = R/d$, the birefringence (or refractive difference) of this sample was determined to be 0.031@550 nm. The single-crystal XRD indicated that the tested crystal plane is (001) (Fig. 4d). The theoretically calculated refractive index dispersion curves from the DFT method (Fig. 4e) showed that $\Delta n_{(001)\text{-plane}}$ (cal.) is 0.023 at 550 nm, which is very close to the experimental value. As suggested by Fig. 4e, the maximal Δn of LSG occurs on the (010) plane with a calculated value of 0.128 at 550 nm. Since it is hard to find a natural (010) plane (the crystals commonly develop as (001) plane, Fig. S4), some fragments were obtained by squashing the (001)-oriented single crystals. We then selected very small fragments with good interference colors to further determine the birefringence (Fig. S5). By doing so, birefringence values of 0.060 and 0.144 at 550 nm were observed. Notably, the latter is very close to the calculated $\Delta n_{(010)\text{-plane}}$ (cal.) = 0.128 at 550 nm. According to these results, LSG exhibits a birefringence of no less than 0.144 at 550 nm. The large birefringence is favorable to trigger a short phase-matching (PM) wavelength. As shown in Fig. 4f, the shortest type I PM wavelength (λ_{PM}) of LSG was estimated to be 262 nm, which also further verified the experimental powder SHG results measured at 532 nm mentioned earlier.

Fig. 4g presents the birefringence comparison of alkaline metal (ammonium) sulfates A_2SO_4 and LSG. The birefringence of LSG is much higher than that of A_2SO_4, and there is a 36-fold enhancement compared to that of Li_2SO_4, highlighting the important role of glycine in improving the birefringence of LSG. For achieving the fourth-harmonic generation of the Nd:YAG laser emitting 1064 nm coherent light, in addition to meeting the sufficiently large birefringence (commonly $\Delta n \geq 0.05$), a wide UV transparency with a cut-off edge ($\lambda_{cut\text{-}off}$) shorter than 266 nm is also inevitably needed. We investigated the Δn and $\lambda_{cut\text{-}off}$ properties of UV-transparent NLO sulfates, and the sulfates satisfying the criteria of $\Delta n \geq 0.05$ are summarized in Fig. 4h; a few sulfates can simultaneously satisfy the two strict conditions. Among them, only $CsSbF_2SO_4$ and $A_2B_4SO_{10}$ (A = NH_4, K, Rb, and Cs) were reported to be phase-matchable at 532 nm.[30,41,60] It should be further noted that LSG exhibits key properties that compete with those of known UV NLO crystals (Fig. 4i and Table S8). Its birefringence (Δn = 0.144@550 nm) is comparable to that of β-BBO

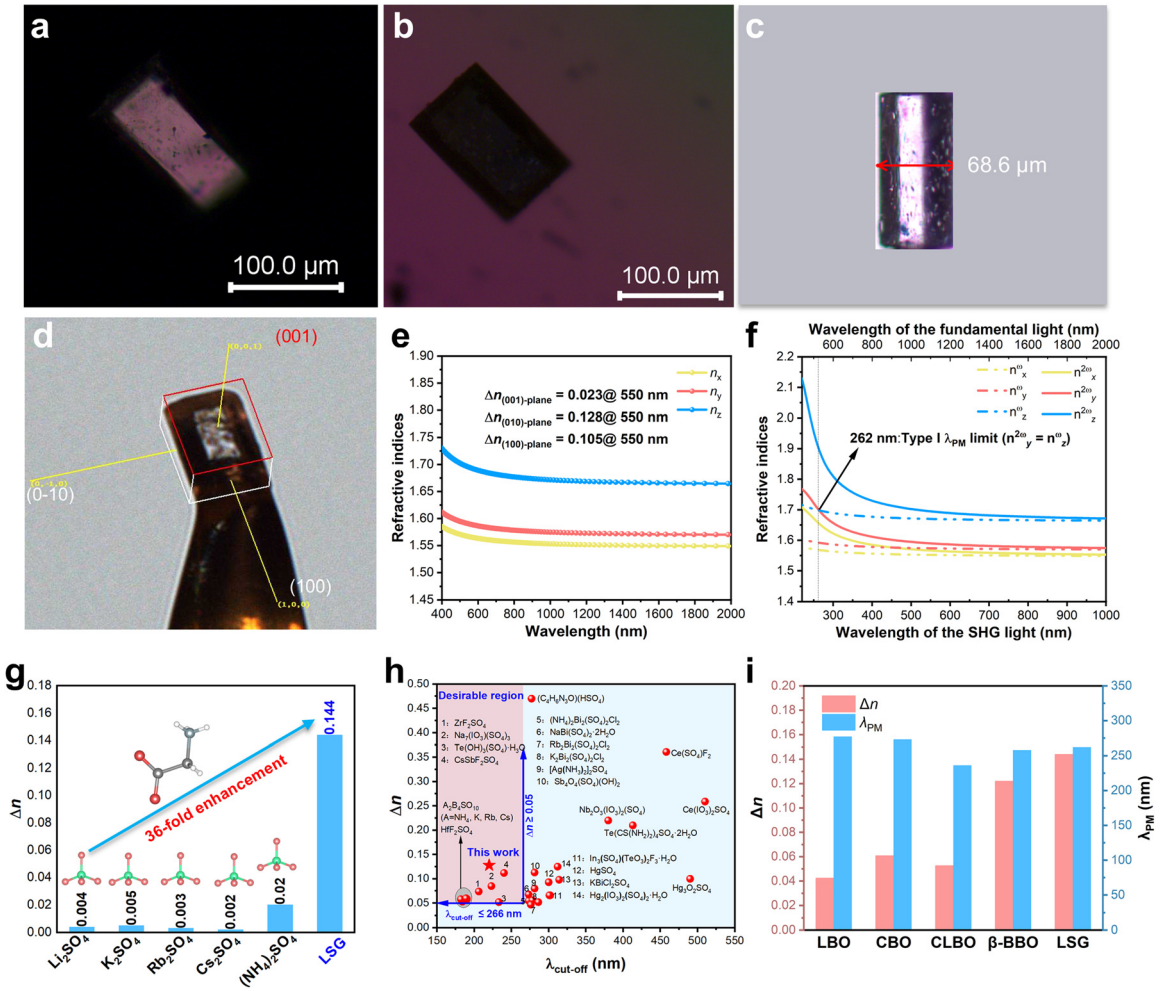

Fig. 4 The birefringence-related properties of LSG. (a) The original interference color of the selected LSG single crystal under cross-polarized light. (b) The complete extinction of the LSG single crystal achieved by the Berek compensator, which gives the retardation (R) values. (c) The thickness of the crystal sample. (d) The crystal plane determination by SCXRD. Birefringence could be determined by the equation $\Delta n = R/d$. (e) The calculated refractive index chromatic dispersion curves. (f) The estimated type-I phase-matching limit (λ_{PM}) based on calculated refractive indices. (g) The birefringence comparison between LSG and A_2SO_4 (A = Li, K, Rb, Cs, and NH_4). (h) The investigation of Δn and $\lambda_{cut\text{-}off}$ of UV-transparent NLO sulfates. Note that a few NLO sulfates are not included since their Δn or $\lambda_{cut\text{-}off}$ data are not available. (i) Comparison of birefringence (Δn) and the shortest PM wavelength (λ_{PM}) of the known UV NLO crystal and LSG.

(Δn = 0.122@546 nm) and is larger than those of LBO (Δn = 0.0424@550 nm), CBO (CsB_3O_5, Δn = 0.0608@546 nm), and CLBO (Δn = 0.0526@532 nm). Additionally, due to the sufficiently large birefringence, its shortest PM wavelength (λ_{PM} = 262 nm) is shorter than those of LBO (λ_{PM} = 277 nm) and CBO (λ_{PM} = 273 nm). These results indicate that LSG has the potential to generate a short-wavelength UV coherent laser (*e.g.*, 266 nm) by a direct SHG process.

Structure–property relationship

To understand the underlying mechanism of the birefringence enhancement of LSG, we first examined the microscopic polarizability anisotropy (δ) of $C_2H_5NO_2$ and compared the results with other groups. As illustrated in Fig. S6, the non-π-conjugated $[SO_4]^{2-}$ and $[PO_4]^{3-}$ with ideal geometry exhibited δ = 0 a.u. while the $C_2H_5NO_2$ molecule exhibited δ up to 19.1 a.u., which is higher than that of π-conjugated $[BO_3]^{3-}$ (δ = 7.1 a.u.) and comparable to those of $[CO_3]^{2-}$ (δ = 12.8 a.u.) and $[NO_3]^{-}$ (δ = 18.4 a.u.). This strongly suggests that the compounds consisting of $C_2H_5NO_2$ have great potential to exhibit large birefringence. The birefringence of LSG (Δn = 0.144 at 550 nm) is comparable to that of several borates, such as $NH_4B_4O_6F$ (Δn = 0.1171 at 1064 nm), $Ca(BO_2)_2$ (Δn = 0.1230–0.1735 at 1529–253 nm), and $Li_2Na_2B_2O_5$ (0.095 at 532 nm), carbonates $NaZnCO_3(OH)$ (Δn = 0.114 at 1064 nm) and $LiZnCO_3(OH)$ (Δn = 0.147 at 1064 nm), as well as the nitrate $La(OH)_2NO_3$ (Δn = 0.146 at 589.6 nm), among others. To gain deep insight into the relationship between electronic characteristics and optical properties of LSG, first-principles calculations based on the DFT method were conducted. The electronic band structure diagram revealed a band gap of 5.25 eV for LSG (Fig. 5a). The partial density of states (PDOS) plots (Fig. 5b) showed that the top of the valence band (approximately −4 to 0 eV) is mainly composed of O-2p, C-2p, H-1s states, while the

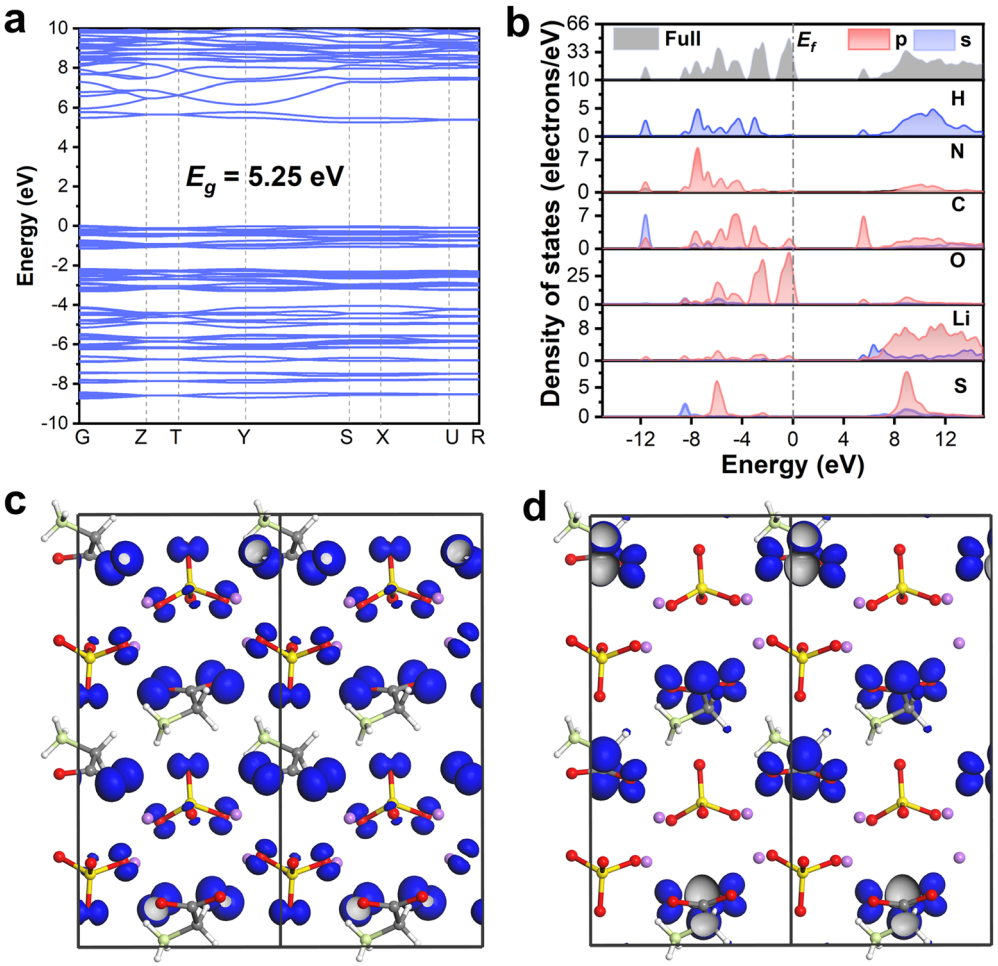

Fig. 5 Theoretical calculations for LSG. (a) Band structure and (b) density of states (DOS). (c) The highest occupied molecular orbitals (HOMO) and (d) lowest unoccupied molecular orbitals (LUMO) of LSG. Purple, yellow, red, pale green, grey, and white represent Li, S, O, N, C, and H atoms, respectively.

bottom of the conduction band (approximately 5.25 to 8 eV) is dominated by C-2p with small amounts of O-2p, Li-2s and 2p orbitals. Fig. 5 shows diagrams of the highest occupied molecular orbitals (HOMO) and lowest unoccupied molecular orbitals (LUMO) of the cell unit of LSG. The HOMO is mainly composed of occupied O-2p states from $C_2H_5NO_2$, as well as $[SO_4]^{2-}$, while the LUMO is dominated by unoccupied O-2p and C-2p states from $C_2H_5NO_2$, suggesting that the electronic activities of O and C atoms from $C_2H_5NO_2$ are crucial for the optical properties exhibited by LSG. Overall, these results indicate that the birefringence enhancement exhibited by LSG is strongly related to the constituent $C_2H_5NO_2$.

Conclusions

In conclusion, enhanced birefringence and extraordinary SHG PM capability have been achieved in a lithium sulfate glycine cocrystal, LSG. The material exhibits a large birefringence value of 0.144@550 nm and a wide UV transparency window with a short $\lambda_{cut\text{-}off}$ of 220 nm. Remarkably, LSG has a short λ_{PM} = 262 nm. Powder SHG measurements revealed that LSG is phase-matchable under both 1064 nm and 532 nm with SHG efficiencies of 0.7 × KDP, and 0.3 × β-BBO, respectively. Moreover, LSG can be thermally stable up to 566 K, which is much more stable than several semi-organic NLO materials; it also shows good air stability and is non-hygroscopic. The structure–property relationship study indicated that the birefringence enhancement of LSG is mainly attributed to the $C_2H_5NO_2$ component. Our findings highlight the effectiveness of using π-conjugated moieties to optimize the key properties of NLO sulfates, providing valuable insight for the development of short-wavelength UV NLO materials.

Author contributions

The manuscript was written through contributions of all the authors. All the authors have given approval to the final version of the manuscript.

Conflicts of interest

The authors declare no conflict of interest.

Data availability

The data supporting this article have been included as part of the SI. Any further relevant data are available from the authors upon reasonable request.

Tables of crystal data and structure refinement, fractional atomic coordinates, anisotropic displacement parameters, selected bond lengths and bond angles, images of as-synthesized single crystals, powder X-ray diffraction patterns, thermogravimetric curve, optical images, birefringence measurement, and polarizability anisotropy of individual groups (PDF). See DOI: **https://doi.org/10.1039/d5tc02204e**

CCDC 2416698 contains the supplementary crystallographic data for this paper.[61]

Acknowledgements

This work acknowledges the National Natural Science Foundation of China (22193042, 22405273), the Natural Science Foundation of Fujian Province (2025J01310365, 2022J02012), the Key Research Program of Frontier Sciences of the Chinese Academy of Sciences (ZDBS-LY-SLH024), the Fujian Institute of Innovation in Chinese Academy of Sciences (FJCXY18010201), and the financial support from the China Postdoctoral Science Foundation (2023M743498).

References

1 C. T. Chen, Y. B. Wang, B. C. Wu, K. C. Wu, W. L. Zeng and L. H. Yu, *Nature*, 1995, **373**, 322–324.
2 M. Mutailipu, K. R. Poeppelmeier and S. Pan, *Chem. Rev.*, 2021, **121**, 1130–1202.
3 G. Zou and K. M. Ok, *Chem. Sci.*, 2020, **11**, 5404–5409.
4 X. Dong, L. Huang and G. Zou, *Acc. Chem. Res.*, 2025, **58**, 150–162.
5 Y. Deng, L. Huang, X. Dong, L. Wang, K. M. Ok, H. Zeng, Z. Lin and G. Zou, *Angew. Chem., Int. Ed.*, 2020, **59**, 21151–21156.
6 D. Göbbels and G. Meyer, *Z. Anorg. Allg. Chem.*, 2003, **629**, 933–935.
7 C. Chen, B. Wu, A. Jiang and G. You, *Sci. Sin., Ser. B*, 1985, **28**, 235–243.
8 C. Chen, Y. Wu, A. Jiang, B. Wu, G. You, R. Li and S. Lin, *J. Opt. Soc. Am. B*, 1989, **6**, 616–621.
9 Z. Lin, J. Lin, Z. Wang, C. Chen and M. H. Lee, *Phys. Rev. B*, 2000, **62**, 1757–1764.
10 H. Wu, S. Pan, K. R. Poeppelmeier, H. Li, D. Jia, Z. Chen, X. Fan, Y. Yang, J. M. Rondinelli and H. Luo, *J. Am. Chem. Soc.*, 2011, **133**, 7786–7790.
11 G. Peng, N. Ye, Z. Lin, L. Kang, S. Pan, M. Zhang, C. Lin, X. Long, M. Luo, Y. Chen, Y. H. Tang, F. Xu and T. Yan, *Angew. Chem., Int. Ed.*, 2018, **57**, 8968–8972.
12 T. Ouyang, Y. Shen and S. Zhao, *Chin. J. Struct. Chem.*, 2023, **42**, 100024.
13 G. Yi and G. Zou, *Chin. J. Struct. Chem.*, 2023, **42**, 100020.
14 X. Liu, L. Kang, P. Gong and Z. Lin, *Angew. Chem., Int. Ed.*, 2021, **60**, 13574–13578.
15 Y. Song, M. Luo, D. Zhao, G. Peng, C. Lin and N. Ye, *J. Mater. Chem. C*, 2017, **5**, 8758–8764.
16 Y. Zhu, J. Gou, C. Yang, Q. Zhu, Y. Xiong and Q. Wu, *Angew. Chem., Int. Ed.*, 2025, e202509290, DOI: **10.1002/anie.202509290**.
17 C. Yang, J. Gou, Y. Zhu, Y. Xiong, Z. Zhu, L. Chen and Q. Wu, *Angew. Chem., Int. Ed.*, 2025, **64**, e202420810.
18 M. Mutailipu, J. Han, Z. Li, F. Li, J. Li, F. Zhang, X. Long, Z. Yang and S. Pan, *Nat. Photonics*, 2023, **17**, 694–701.
19 H. Qiu, F. Li, C. Jin, Z. Yang, J. Li, S. Pan and M. Mutailipu, *Angew. Chem., Int. Ed.*, 2024, **63**, e202316194.
20 Y.-G. Chen, X. Hu, Y. Guo, S. Zhao, B. Zhang, X. Zhang and X.-M. Zhang, *Chem. Mater.*, 2024, **36**, 4775–4781.
21 P. H. Guo, X. Zhang, Y. Guo, N. Zhang, Y. G. Chen, X. Jiang, Z. Lin and X. M. Zhang, *Angew. Chem., Int. Ed.*, 2025, e202508997, DOI: **10.1002/anie.202508997**.
22 X. Chen, Y. Li, J. Luo and S. Zhao, *Chin. J. Struct. Chem.*, 2023, **42**, 100044.
23 Y. C. Yang, X. Liu, J. Lu, L. M. Wu and L. Chen, *Angew. Chem., Int. Ed.*, 2021, **60**, 21216–21220.
24 Z. Geng, R. Fu, Z. Ma and X. Wu, *Adv. Opt. Mater.*, 2024, **12**, 2401332.
25 Y. Li, F. Liang, S. Zhao, L. Li, Z. Wu, Q. Ding, S. Liu, Z. Lin, M. Hong and J. Luo, *J. Am. Chem. Soc.*, 2019, **141**, 3833–3837.
26 Q. Wei, C. He, K. Wang, X. F. Duan, X. T. An, J. H. Li and G. M. Wang, *Chem. – Eur. J.*, 2021, **27**, 5880–5884.
27 C. Wu, X. Jiang, Y. Hu, C. Jiang, T. Wu, Z. Lin, Z. Huang, M. G. Humphrey and C. Zhang, *Angew. Chem., Int. Ed.*, 2022, **61**, e202115855.
28 Y. Li, Z. Zhou, S. Zhao, F. Liang, Q. Ding, J. Sun, Z. Lin, M. Hong and J. Luo, *Angew. Chem., Int. Ed.*, 2021, **60**, 11457–11463.
29 Y. Song, H. Yu, B. Li, X. Li, Y. Zhou, Y. Li, C. He, G. Zhang, J. Luo and S. Zhao, *Adv. Funct. Mater.*, 2023, **34**, 2310407.
30 X. Dong, L. Huang, C. Hu, H. Zeng, Z. Lin, X. Wang, K. M. Ok and G. Zou, *Angew. Chem., Int. Ed.*, 2019, **58**, 6528–6534.
31 K. Chen, Y. Yang, G. Peng, S. Yang, T. Yan, H. Fan, Z. Lin and N. Ye, *J. Mater. Chem. C*, 2019, **7**, 9900–9907.
32 Y. Han, X. Zhao, F. Xu, B. Li, N. Ye and M. Luo, *J. Alloys Compd.*, 2022, 902.
33 X. Dong, L. Huang, H. Zeng, Z. Lin, K. M. Ok and G. Zou, *Angew. Chem., Int. Ed.*, 2022, **61**, e202116790.
34 C. Wu, C. Jiang, G. Wei, X. Jiang, Z. Wang, Z. Lin, Z. Huang, M. G. Humphrey and C. Zhang, *J. Am. Chem. Soc.*, 2023, **145**, 3040–3046.
35 C. Wu, T. Wu, X. Jiang, Z. Wang, H. Sha, L. Lin, Z. Lin, Z. Huang, X. Long, M. G. Humphrey and C. Zhang, *J. Am. Chem. Soc.*, 2021, **143**, 4138–4142.
36 P. F. Li, C. L. Hu, Y. F. Li, J. G. Mao and F. Kong, *J. Am. Chem. Soc.*, 2024, **146**, 7868–7874.
37 W. Jin, W. Zhang, A. Tudi, L. Wang, X. Zhou, Z. Yang and S. Pan, *Adv. Sci.*, 2021, **8**, e2003594.
38 X. Hao, M. Luo, C. Lin, G. Peng, F. Xu and N. Ye, *Angew. Chem., Int. Ed.*, 2021, **60**, 7621–7625.

39 X. Wang, X. Leng, Y. Kuk, J. Lee, Q. Jing and K. M. Ok, *Angew. Chem., Int. Ed.*, 2024, **63**, e202315434.
40 H. Tian, C. Lin, X. Zhao, F. Xu, C. Wang, N. Ye and M. Luo, *CCS Chem.*, 2023, **5**, 2497–2505.
41 Z. Li, W. Jin, F. Zhang, Z. Chen, Z. Yang and S. Pan, *Angew. Chem., Int. Ed.*, 2022, **61**, e202112844.
42 Z. Bai and K. M. Ok, *Angew. Chem., Int. Ed.*, 2023, e202315311, DOI: 10.1002/anie.202315311,.
43 Z. Bai, J. Lee, C. L. Hu, G. Zou and K. M. Ok, *Chem. Sci.*, 2024, **15**, 6572–6576.
44 M. R. Suresh Kumar, H. J. Ravindra and S. M. Dharmaprakash, *J. Cryst. Growth*, 2007, **306**, 361–365.
45 O. V. Dolomanov, L. J. Bourhis, R. J. Gildea, J. A. K. Howard and H. Puschmann, *J. Appl. Crystallogr.*, 2009, **42**, 339–341.
46 G. M. Sheldrick, *Acta Crystallogr.*, 2015, **A71**, 3–8.
47 G. M. Sheldrick, *Acta Crystallogr.*, 2015, **C71**, 3–8.
48 A. L. J. Spek, *J. Appl. Crystallogr.*, 2003, **36**, 7–13.
49 S. Landi Jr, I. R. Segundo, E. Freitas, M. Vasilevskiy, J. Carneiro and C. J. Tavares, *Solid State Commun.*, 2022, **341**, 114573.
50 M. D. Segall, P. J. Lindan, M. A. Probert, C. J. Pickard, P. J. Hasnip, S. J. Clark and M. C. Payne, *J. Phys.: Condens. Matter*, 2002, **14**, 2717–2744.
51 J. P. Perdew, K. Burke and M. Ernzerhof, *Phys. Rev. Lett.*, 1996, **77**, 3865–3868.
52 G. W. T. M. J. Frisch, H. B. Schlegel, G. E. Scuseria, M. A. Robb, J. R. Cheeseman, G. Scalmani, V. Barone, B. Mennucci, G. A. Petersson, H. Nakatsuji, M. Caricato, X. Li, H. P. Hratchian, A. F. Izmaylov, J. Bloino, G. Zheng, J. L. Sonnenberg, M. Hada, M. Ehara, K. Toyota, R. Fukuda, J. Hasegawa, M. Ishida, T. Nakajima, Y. Honda, O. Kitao, H. Nakai, T. Vreven, J. A. Montgomery Jr., J. E. Peralta, F. Ogliaro, M. Bearpark, J. J. Heyd, E. Brothers, K. N. Kudin, V. N. Staroverov, T. Keith, R. Kobayashi, J. Normand, K. Raghavachari, A. Rendell, J. C. Burant, S. S. Iyengar, J. Tomasi, M. Cossi, N. Rega, J. M. Millam, M. Klene, J. E. Knox, J. B. Cross, V. Bakken, C. Adamo, J. Jaramillo, R. Gomperts, R. E. Stratmann, O. Yazyev, A. J. Austin, R. Cammi, C. Pomelli, J. W. Ochterski, R. L. Martin, K. Morokuma, V. G. Zakrzewski, G. A. Voth, P. Salvador, J. J. Dannenberg, S. Dapprich, A. D. Daniels, O. Farkas, J. B. Foresman, J. V. Ortiz, J. Cioslowski and D. J. Fox, *Gaussian 09W*, Gaussian, Inc., Wallingford CT, 2016.
53 J. Lu, X. Liu, M. Zhao, X. B. Deng, K. X. Shi, Q. R. Wu, L. Chen and L. M. Wu, *J. Am. Chem. Soc.*, 2021, **143**, 3647–3654.
54 C. Jin, H. Zeng, F. Zhang, H. Qiu, Z. Yang, M. Mutailipu and S. Pan, *Chem. Mater.*, 2021, **34**, 440–450.
55 M. Luo, C. Lin, D. Lin and N. Ye, *Angew. Chem., Int. Ed.*, 2020, **59**, 15978–15981.
56 W. Yang, L. Liu, L. Zhang, Y. Huang, F. Yuan and Z. Lin, *Cryst. Growth Des.*, 2023, **23**, 5614–5620.
57 W. Huang, X. Zhang, Y. Li, Y. Zhou, X. Chen, X. Li, F. Wu, M. Hong, J. Luo and S. Zhao, *Angew. Chem., Int. Ed.*, 2022, **61**, e202202746.
58 Y. Li, X. Zhang, J. Zheng, Y. Zhou, W. Huang, Y. Song, H. Wang, X. Song, J. Luo and S. Zhao, *Angew. Chem., Int. Ed.*, 2023, **62**, e202304498.
59 Y. Li, X. Zhang, Y. Zhou, W. Huang, Y. Song, H. Wang, M. Li, M. Hong, J. Luo and S. Zhao, *Angew. Chem., Int. Ed.*, 2022, **61**, e202208811.
60 Z. Li, W. Jin, F. Zhang,. Yang and S. Pan, *ACS Cent. Sci.*, 2022, **8**, 1557–1564.
61 Z. Bai, S. Chen, X. Chen, Y. Wang, X. Zhou, Y. Song, Y. Li, S. Zhao and J. Luo, CCDC 2416698: Experimental Crystal Structure Determination, 2025, DOI: 10.5517/ccdc.csd.cc2m3s0k.